LA-UR-81-1045

TITLE: CAN MAGNETIC REFRIGERATORS LIQUEFY HYDROGEN AT HIGH EFFICIENCY?

MASTER

AUTHOR(S): J. A. Barclay

SUBMITTED TO: 1981 National Heat Transfer Conference, Special Session of Liquid Hydrogen as a Fuel, Milwaukee, WI, Aug. 2-5, 1981

DISCLAIMER

By acceptance of this article, the publisher recognizes that the U.S. Government retains a nonexclusive, royalty-free license to publish or reproduce the published form of this contribution, or to allow others to do so, for U.S. Government purposes.

The Los Alamos Scientific Laboratory requests that the publisher identify this article as work performed under the auspices of the U.S. Department of Energy

University of California

LOS ALAMOS SCIENTIFIC LABORATORY
Post Office Box 1663 Los Alamos, New Mexico 87545
An Affirmative Action/Equal Opportunity Employer

Form No. 836 R3
St. No. 2629
12/78

UNITED STATES
DEPARTMENT OF ENERGY
CONTRACT W-7405-ENG. 36

CAN MAGNETIC REFRIGERATORS LIQUEFY HYDROGEN AT HIGH EFFICIENCY?*

J. A. Barclay
Group P-10, MS-764
Los Alamos National Laboratory
Los Alamos, New Mexico 87545

Abstract

A concept for a hydrogen liquefier based on the magnetocaloric effect is introduced. A second-law analysis of the general device is described. The calculation predicts that efficiencies ∿ 50% of Carnot are probable. A brief comparison to gas refrigeration systems is made.

*The work was performed under the auspices of the U. S. Department of Energy.

NOMENCLATURE

A_c - contact area, m^2
B - magnetic field, T
B_J - Brillouin function, dimensionless
C_B - heat capacity at constant field, J/kgK
C_o - heat capacity at zero field, J/kgK
C_p - heat capacity at constant pressure, J/kgK
D - demagnetizing factor, dimensionless
G - molecular weight, kg/mole
J - total electronic angular momentum operator, dimensionless
L - length, m
M - magnetization, Am^2/mole
N - Avogadro's number, $mole^{-1}$
N_{tu} - number of heat transfer units, dimensionless
ΔP - pressure drop, Pa
Q_c - cooling power, W
Q_h - heat rejection power, W
S - entropy, J/mole K
ΔS - rate of reversible entropy change, W/Km^3
ΔS_{IRR} - rate of irreversible entropy production, W/Km^3
T - temperature, K
T_c - cold-bath temperature, K
T_h - hot-bath temperature, K
T_{IN} - inlet temperature, K
T_{OUT} - outlet temperature, K

T_o - Curie temperature, K
$\bar{T}$ - average temperature, K
ΔT - magnetocaloric adiabatic temperature change, K
ΔT_{GS} - gas to solid temperature difference, K
V - volume, m^3
$\dot{V}$ - volume flow rate, m^3/s
x - argument of Brillouin function, dimensionless
d_p - particle diameter, m
g - Lande g-factor, dimensionless
h - conductance, W/m K
k - Boltzmann constant, J/K
$\dot{m}$ - mass flow rate, kg/s
q - heat flux vector, W/m^2
v - velocity, m/s
α - porosity, dimensionless
β - Bohr magneton J/T
η - efficiency, dimensionless
κ - fluid thermal conductivity, W/mK
λ - effective thermal conductivity, W/mK
λ_o - molecular field constant, dimensionless
μ - viscosity, Pas
μ_o - permability constant, Wb/Am
ρ - density, kg/m^3

INTRODUCTION

Hydrogen has been suggested as a fuel for cars, trains, buses and airplanes. If hydrogen is used as a liquid, the liquefaction process adds considerably to the cost. One of the conclusions from analyses of the cost of liquid hydrogen production[1-5] is that about half of the cost is from the feed supply and the other half from the liquefaction process. Another very important conclusion from these reports is that while liquid hydrogen appears to be an excellent fuel, it costs too much at the present time to be the logical choice for rapid development. However, if the cost of liquefaction were significantly reduced, the choice of fuels may swing in favor of liquid hydrogen. All of the present methods of liquefaction of liquid hydrogen as well as of other cryogens are based on gas refrigeration methods in which gas is compressed in one part of the cycle, in order to reject heat from the gas, and then expanded in another part of the cycle to cool and, eventually, to liquefy the gas. Several studies of the efficiency of gas-based refrigerators

for cryogens have been published.[6-9] The main sources of inefficiency are the room-temperature compressors, with their associated aftercoolers, and the gas expanders. All of the efficiency studies agree that about 35-40% of Carnot efficiency (ideal) is the best that is now possible for existing cycles, even for very large plants, and that the prospect is very poor for much improvement. Therefore, if liquefaction costs for the large-scale production of liquid hydrogen, helium and liquid natural gas are to be significantly reduced, a new refrigeration technology must be found.

The purpose of this paper is to describe the concept of magnetic refrigeration, to show that a refrigerator based on this concept should be able to produce liquid hydrogen at ~ 50% of Carnot, and to briefly discuss the results in comparison to gas refrigerators.

PRINCIPLES OF MAGNETIC REFRIGERATION

Magnetocaloric Effect

Magnetic refrigerators exploit the temperature and magnetic field dependence of the magnetic entropy of a solid material to extract heat from a low temperature source and transfer it to a higher-temperature sink. The entropy change relevant to these processes is given by

$$dS = \left(\frac{\partial M}{\partial T}\right)_B dT + \left(\frac{\partial S}{\partial B}\right)_T dB = \frac{C_B}{T} dT + \left(\frac{\partial M}{\partial T}\right)_B dB \quad , \qquad (1)$$

where S is entropy, B is magnetic field, C_B is heat capacity at constant magnetic field, M is magnetization, and T is absolute temperature. Thus, in order to predict the isothermal entropy change or the adiabatic temperature change with magnetic field variation, the zero-magnetic-field heat capacity C_0 and the equation of state of the magnetization are required. The magnetic field-dependent heat capacity can be obtained by using

$$C_B = C_0 + T \int_0^B \left(\frac{\partial^2 M}{\partial T^2}\right)_B dB \quad . \qquad (2)$$

The equation of state for paramagnets and ferromagnets is given by

$$M(B,T) = M_s B_J(x) \quad , \qquad (3)$$

where M_s is the saturation magnetization and $B_J(x)$ is the Brillouin function. For a paramagnet

$$x = g\beta BJ/kT \quad , \qquad (4)$$

where g is the Lande g-factor, β the Bohr magneton, J the total electronic angular momentum operator, and k the Boltzmann constant. For a ferromagnet, in the molecular-field approximation,

$$x = g\beta J[B - (D\mu_0\rho/G)M + (\lambda_0\rho\mu_0/G)M]/kT \quad , \qquad (5)$$

where D is the demagnetizing factor, μ_0 is the permeability constant, ρ is the density, G is the molecular weight, and λ_0 the molecular field constant given by

$$\lambda_0 = 3kT_0G/N\rho\mu_0 g^2\beta^2 J(J+1) \quad , \qquad (6)$$

with T_0 equal to the Curie temperature. Substitution of Eqs. (5) and (6) into (3) gives a transcendental equation for M, which can be solved by iteration. Paramagnets at low temperature (1-20 K) and ferromagnets near their Curie temperature (20-300 K) show appreciable entropy changes with field; values range from $\geq$1R at low temperatures to 0.1-0.2R at room temperature with a maximum of $R\ln(2J+1)$, where R is the gas constant. For small x, Eq. (3) can be expanded and substituted into Eq. (1) to correctly predict the normal magnetocaloric effect, i.e., the increase in temperature of a paramagnetic solid when adiabatically magnetized.

Thermodynamic Cycles for Magnetic Refrigerators

In order to use the magnetocaloric effect in a refrigerator a suitable thermodynamic cycle must be completed. The magnetic analogues of several gas cycles exist and will be discussed separately.

Carnot cycle. This historic cycle consists of 2 isothermal steps and 2 isentropic steps and is easy to execute in a magnetic system. Consider a ferromagnetic material near its Curie temperature such that the material can be isolated from or put in contact with hot and cold baths at will. The first stage of this cycle is an isothermal magnetization while in contact with the hot bath; the heat of magnetization is rejected into the hot bath. Next, an isolated (adiabatic), partial demagnetization is performed which cools the material to a lower temperature. The third step puts the material in contact with the cold bath as the demagnetization is continued to zero field; heat is drawn from the cold bath. The final step of the cycle is an adiabatic partial magnetization back to the original starting temperature. These two isothermal steps and two adiabatic steps as described constitute a magnetic Carnot cycle. The temperature span of a Carnot cycle is limited to 5-10 K with a ~ 10-T field change but no regeneration is required. If larger temperature spans are required other cycles can be used. A Carnot cycle is illustrated in Fig. 1.

Brayton cycle. This magnetic cycle consists of two adiabatic steps and two isofield steps. It requires regeneration but can cover much larger temperature spans than a Carnot cycle. The Brayton cycle is very attractive because of the natural way of coupling to the external heat exchangers through the temperature change caused by the ad[illegible] field changes, as illustrated in Fig. 1.

Other possible cycles. Magnetic Ericsson and Stirling cycles are also possible. Ericsson cycles consist of two isothermal steps and two isofield steps. Stirling cycles require two isothermal steps and two isomagnetization steps. Both of these cycles require regeneration but can span large temperature differences. Because these cycles require excellent heat transfer between the heat-exchange fluid and the source and sink to obtain the isothermal steps, the Brayton cycle tends to be easier to implement in a practical device.

Configuration of a Magnetic Refrigerator.

In order to make an operating refrigerator capable of executing one of the cycles discussed in the previous section of this paper, a number of requirements must be met. First of all, depending on the temperature span, suitable magnetic material or materials must be selected. If the temperature span is ~40 K or

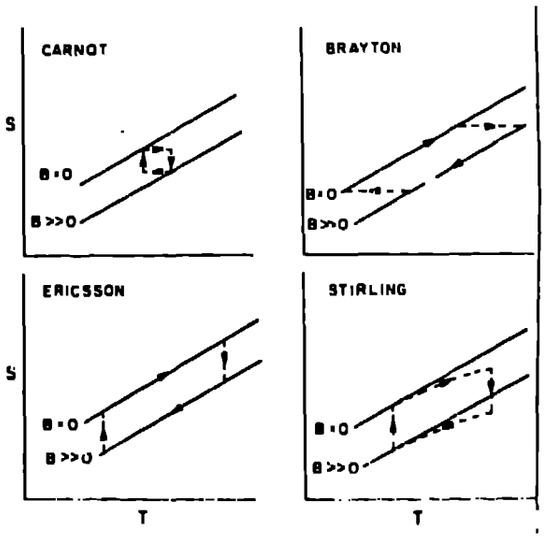

Fig. 1. The most feasible magnetic cycles that can be used to make a refrigerator based on the magnetocaloric effect.

less, a single material will suffice. If a larger temperature span is required, then a series of materials must be used such that each material operates near its Curie temperature. Second, a heat-exchange fluid must be selected in order to couple the magnetic solid to the hot and cold heat exchangers and to effect the regeneration. A magnet and Dewar are necessary components along with a source of power to provide the work required for the refrigeration cycle. For a small temperature span, ≤40 K, there are several possible combinations of the required components; but for larger spans, such as 20–300 K, there are fewer possible configurations that might work. The basis of one such configuration of refrigerator is called active magnetic regeneration. This concept is explained in the next section.

ACTIVE MAGNETIC REGENERATOR FOR 20–300 K

The active magnetic regenerator is a device composed of several magnetic materials that are thermodynamically cycled to provide refrigeration over an extended temperature range. The basic theory is that of an ordinary regenerator except that the temperature of the materials can be changed by the application or removal of a magnetic field and that a coupled thermal wavefront propagates back and forth in the regenerator.

Each different material executes a small Brayton cycle near its Curie temperature but when all of the materials are combined, they yield a Brayton cycle from 20 to 300 K. The basic cycle is illustrated in Fig. 2 and is described as follows. Consider a porous-bed regenerator composed of a series of different ferromagnetic materials with T_C gradually decreasing from the hot-bath temperature T_H to the cold-bath temperature T_C. Also consider that temperature gradient is nearly uniform but displaced to the left of the center in the regenerator, as shown in the top frame of Fig. 2. (For start up from a warm condition, i.e., T_H everywhere, it takes several cycles to reach the condition assumed above, so for simplicity we start with the temperature gradient established.) Upon application of a magnetic field, the temperature rise along the bed will adiabatically increase by ΔT which is about 15–20 K for a 10-T field. (One of the characteristics of magnetic refrigerants is that ΔT is roughly independent of T if the material is near its Curie temperature.) After the field is applied, helium or hydrogen gas, at temperature T_C is pushed through the bed from the cold end, which is now at $T_C + \Delta T$. As the gas at T_C enters the bed, the gas will warm as the bed cools, and a thermal wavefront of magnitude ΔT will be established as shown in the middle frame of Fig. 2. The overall wavefront of magnitude $(T_H + \Delta T - T_C)$ will propagate through the regenerator (to the right in the middle frame of Fig. 2) as gas continues to flow into the bed at T_C. The gas leaves the regenerator at $T_H + \Delta T$ until the thermal wavefront arrives at the hot end of the regenerator, at which time the temperature of the exiting gas drops to T_H. When this happens, the gas flow is stopped and the regenerator is adiabatically demagnetized. The temperatures all along the bed drop by ΔT, as shown in frame 4 of Fig. 2, in preparation for the reverse flow of gas. The gas that came out of the regenerator at $T_H + \Delta T$ during the magnetized

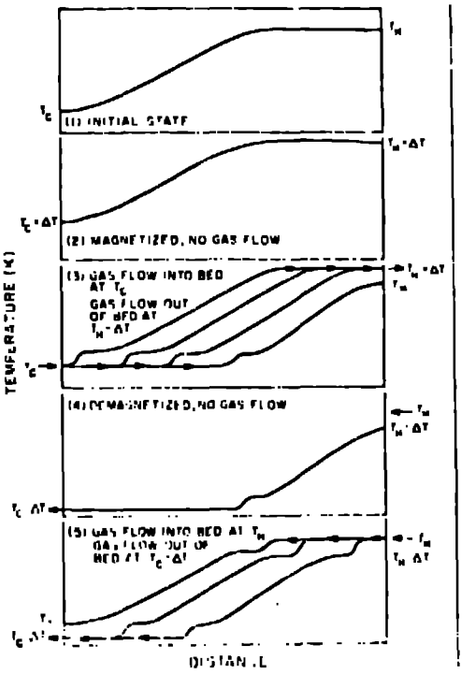

Fig. 2. Active-magnetic regenerative refrigeration cycle showing the thermal wavefront propagation back and forth through the regenerator.

stage is put through a heat exchanger and cooled to T_H before it is pushed back into the regenerator after demagnetization. Another complex thermal wave of magnitude $[T_H - (T_C - \Delta T)]$ is established; but it travels in the opposite direction to the first thermal wavefront, as shown in the bottom frame of Fig. 2.

The gas exits the cold end at T_C-ΔT and is put in contact with a load to be heated to T_C. When the gas temperature at the cold end of the regenerator increases from T_C-ΔT to T_C, the gas flow is stopped and the cycle now repeats as the regenerator is again magnetized.

The cooling capacity of a magnetic regenerative refrigerator is given by

$$\dot{Q}_C = \dot{m} C_p \Delta T_C \quad , \tag{7}$$

where ΔT_C is the adiabatic temperature change of the magnetic materials, $\dot{m}$ the gas flow rate, and C_p the heat capacity of the gas at constant pressure. The exhaust hot gas can reject heat at a rate given by

$$\dot{Q}_H = \dot{m} C_p \Delta T_H \quad , \tag{8}$$

where ΔT_H is the adiabatic temperature change of the magnetic material at the hot end. $\dot{Q}_H$ and $\dot{Q}_C$ are ideally related to the ratio of T_H to T_C; in the ideal case this relation is

$$\dot{Q}_H = \left(\frac{\bar{T}_H}{\bar{T}_C}\right)\dot{Q}_C \quad , \tag{9}$$

where $\bar{T}_H$ is $T_H + \Delta T_H/2$ and $\bar{T}_C$ is $T_C - \Delta T_C/2$. Consider a cylindrical, regenerative bed with gas flowing in one end and only out of the other end. In this case $\dot{m}$ will change according to the continuity equation (ρ and, therefore, v will also change), C_p is approximately constant, and the combination of Eqs. (7), (8), and (9) gives the relationship

$$\frac{\bar{T}_H}{\bar{T}_C} = \frac{\Delta T_H \dot{m}_H}{\Delta T_C \dot{m}_C} \quad , \tag{10}$$

where $\dot{m}_H$ and $\dot{m}_C$ are the mass flow rates at the hot and cold ends, respectively. The relationship in Eq. (10) could be accommodated by changing the magnetic field across the bed until ΔT_C is the correct fraction of ΔT_H. The sculpturing of the magnetic field is a very advantageous extra degree of freedom in magnetic systems. The constraint of Eq. (10) is caused by C_p being constant and shows how the heat-rejection rate at room temperature limits the cooling power of the colder regions of the magnetic refrigerator. It is desirable to overcome the constraint of Eq. (10) because the colder materials have a larger entropy change than those near room temperature, and the larger entropy change could be used advantageously. The way to remove the constraint is to vary $\dot{m}$ along the cylinder so that the full $\Delta T_C \sim \Delta T_H \sim 1^5$ K (and the full entropy change) can be used in a much more economical way. As we shall show later, varying $\dot{m}$ along the temperature span is a natural requirement for a liquefier.

MAGNETIC LIQUEFIER DESIGN

An active magnetic regenerative refrigerator can be the basis of a device potentially capable of liquefying hydrogen. The limiting factors in this concept are the simultaneous requirements of excellent heat transfer in a porous bed with minimum pressure drop. In addition, the diffusive mixing of the heat transfer fluid may be a problem. Thermal addenda must be minimized at the same time that the magnetic forces are handled. There are many factors associated with the above design criteria that need to be investigated before any particular design is chosen for development. However, to indicate that there are indeed possibilities, a basic concept is discussed.

When a refrigerator is converted to a liquefier, design changes occur because the feed gas to be liquefied has to be cooled from room temperature to the liquefaction temperature. In order to do this efficiently, the cooling must be done over as wide a temperature span as possible, i.e., ideally, continuously from room temperature downwards. In the case of hydrogen there is an additional thermal load that comes from the ortho to para conversion, the best case being maintenance of the equilibrium ratio at any temperature. Unfortunately, half of the ortho-para conversion heat will be produced below 77 K and must be taken into account in the liquefier design. Magnetic liquefiers based on active magnetic regeneration should be able to have balanced flow during the cycle by using a separate working gas and liquefying gas. The constraint associated with mass flow rate change discussed earlier can also be utilized beneficially in a magnetic liquefier.

A basic, potential liquefier process is schematically shown in Fig. 3. The operation of each of the four stages is as described in the third section on the descriptive theory of the activemagnetic regenerator. The process in Fig. 3 shows some mass flow being diverted after stages 1, 2, and 3. This diversion allows the cooling of the incoming feed hydrogen and allows the mass flow to be different in each stage for more economical use of the magnetic material. The reciprocating nature of the process in Fig. 3 requires valves and reservoirs in various locations to control the gas flow through the proper sequence as the materials move in and out of the magnetic field. Design calculations for a schematic magnetic liquefier of Fig. 3 that is capable of producing $\sim$ 0.7 ℓ/h liquid hydrogen at 20.4 K indicate an overall efficiency of 54% of Carnot, a volume of $\sim$ 76 ℓ ($7.6 \times 10^{-2} m^3$) and a mass of 160 kg, including magnetic shielding around the Dewar. The additional parasitic cooling at 20 K due to the requirement of maintaining 4.2 K helium for the superconducting magnet is estimated as 120 mW. This additional load has a negligible effect on the liquefier overall efficiency. The statements above are justified in the next section.

PARAMETRIC ANALYSIS AND EFFICIENCY CALCULATION

Although there are several features of magnetic refrigeration that render it worthy of development, the most significant of these is the potential for improved efficiency. In order to estimate just how high the efficiency of a magnetic liquefier might be, a parametric analysis on a hypothetical system was performed. The design used is schematically shown in Fig. 3, i.e., a four-stage magnetic liquefier. Consider each stage to consist of a

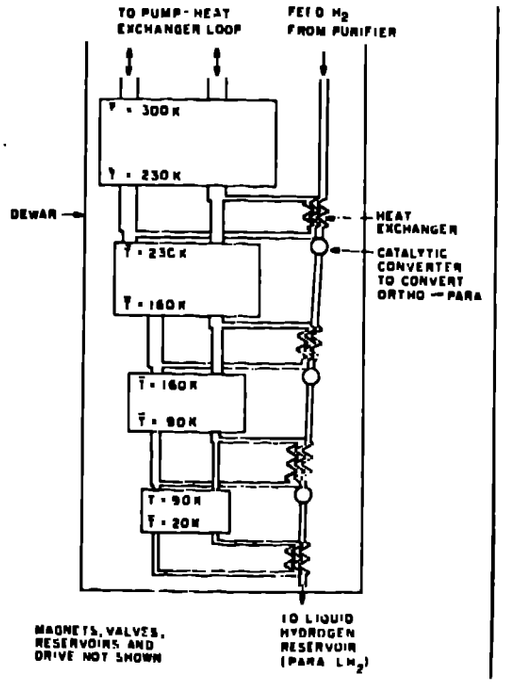

Fig. 3. Schematic diagram of a reciprocating-type magnetic liquefier for hydrogen that uses the Brayton cycle.

porous-bed regenerator made from a stack of magnetic materials with T_0 appropriately varying along the bed. Also consider the stages to span equally the temperature range from 20 to 100 K, i.e., 20 K in each stage.

The efficiency η in this concept is defined in the ratio of the real coefficient of performance to the ideal coefficient of performance, given by

$$\eta = \frac{(\Delta\dot{S}_{II} - \Delta\dot{S}_{IRR})T_C}{T_H\Delta\dot{S}_{II} - (\Delta\dot{S}_{II} - \Delta\dot{S}_{IRR})T_C} = \frac{\Delta\dot{S}_{II}T_C}{T_H\Delta\dot{S}_{II} - T_C\Delta\dot{S}_{II}}$$

$$= \frac{(T_H - T_C)\left(1 - \dfrac{\Delta\dot{S}_{IRR}}{\Delta\dot{S}_{II}}\right)}{T_H - \left(1 - \dfrac{\Delta\dot{S}_{IRR}}{\Delta\dot{S}_{II}}\right)T_C} \quad . \tag{11}$$

Here $\Delta\dot{S}_{IRR}$ is the rate of irreversible entropy production and $\Delta\dot{S}_{II}$ is the rate of reversible, high-temperature entropy change caused by the magnetic field during the thermodynamic cycle. From Eq. (11) it is clear that $\Delta\dot{S}_{IRR}/\Delta\dot{S}_{II}$ needs to be calculated in order to determine the efficiency of each stage and, hence, for the liquefier. Because there are several types of unavoidable sources of $\Delta\dot{S}_{IRR}$, the larger $\Delta\dot{S}_{II}$ the better the chance of obtaining higher efficiency. Therefore, the maximum field change that is practical should be used on the magnetic materials that have the largest magnetization. Rare earth compounds tend to have the largest possible magnetizations and either Nb-Ti or Nb_3Sn superconductors can be used to produce high-field (10 T) magnets.

The major sources of irreversible entropy in this system are given by

$$\Delta\dot{S}_{IRR}\ (\text{Total}) = \Delta\dot{S}_{IRR}\ (\text{Conduction + Mixing}) + \Delta\dot{S}_{IRR}\ (\text{Flow Loss}) + \Delta\dot{S}_{IRR}\ (\text{Internal Heat Transfer}) + \Delta\dot{S}_{IRR}\ (\text{Heat Exchange}) + \Delta\dot{S}_{IRR}\ (\text{Miscellaneous}) \tag{12}$$

We consider each term in Eq. (12) separately.

The first source of irreversible entropy in the regenerative bed is conduction through the bed due to the temperature gradients in the bed. As shown in Fig. 3, there is a complex temperature profile in the thermal wavefront, but it can be approximately decomposed into three temperature gradients in the regenerative bed; one from T_H to T_C over the length of the bed, and the others across ΔT over a fraction of the bed length. The irreversible entropy production rate from heat flow across a temperature gradient can be calculated by[10]

$$\Delta\dot{S}_{IRR} = \frac{-q\cdot\nabla T}{T^2} \quad , \tag{13}$$

where q is the heat flux vector and ∇ is the gradient operator. The heat flow can be expressed in terms of the Fourier expression

$$q = -\lambda\nabla T \quad , \tag{14}$$

where λ is the effective thermal conductivity of the bed; hence, rate of irreversible entropy per unit volume of the bed is given by

$$\Delta\dot{S}_{IRR} = \frac{\lambda(\nabla T)^2}{T^2} \quad . \tag{15}$$

The ratio of $\Delta\dot{S}_{IRR}$ to $\Delta\dot{S}_{II}$ is required; the relevant ΔS in the refrigerator is that at the cold end, which, however, is limited by $\Delta\dot{S}_{II}$ at the hot end of the regenerator because of energy conservation mass flow changes in the heat-exchange gas, as explained in an earlier section. Therefore, per unit volume,

$$\Delta\dot{S}_{II} = \dot{m}C_p\Delta T_{II}/(\bar{T}_{II}V) \tag{16}$$

where $\dot{m}C_p$ is the thermal mass flux of the heat-exchange fluid, ΔT_{II} the adiabatic temperature change of the magnetic material at the hot end of the regenerator, V is the bed volume, and $\bar{T}_{II}$ is the average hot-end temperature. Combining Eqs. (15) and (16) leads to the following result:

$$\frac{\Delta\dot{S}_{IRR}}{\Delta\dot{S}_{II}}\left(\begin{matrix}\text{conduction}\\ \text{and}\\ \text{mixing}\end{matrix}\right) = \frac{\lambda(T_{II} - T_C)^2\,\bar{T}_{II}}{\bar{T}^2\dot{m}C_p\Delta T_{II}}$$

$$+ \frac{36\lambda\Delta T_{II}\bar{T}_{II}}{L\bar{T}^2\rho vC_p} + \frac{36\lambda\Delta\bar{T}_{II}^2T_C}{\bar{T}_{II}L\bar{T}^2\rho vC_p} \tag{17}$$

where $\bar{T}$ is the mean temperature and $\dot{m}$ has been replaced by $\rho vV/L$.

The first term in Eq. (17) is the contribution from the overall gradient across the whole regenerator length, and the second and third terms are the contributions from the ΔT temperature changes, estimated to occur over one-sixth of the bed length. The effective thermal conductivity is a combination of static bed conductivity and diffusive mixing of the fluid. Generally, a value of $\lambda \sim 0.1$ to 1 W/mK has been reasonable in analysis of our room-temperature porous-bed experiments. This parameter should decrease in value as the temperature decreases.

The second source of irreversible entropy production comes from the dissipation of the kinetic energy of the heat-exchange fluid in the porous bed. The pressure drop in porous beds is well described by Ergun's equation.[11] The irreversible entropy produced is

$$\dot{\Delta S}_{IRR}\ (\text{Flow}) = \frac{\Delta P \dot{V}}{\bar{T}} \quad . \tag{18}$$

If Ergun's equation is combined with Eqs. (16) and (18), the result is

$$\frac{\dot{\Delta S}_{IRR}}{\dot{\Delta S}_H}\ (\text{Flow}) = 2.5\left[\frac{150\mu(1-\alpha)}{d_p \rho v} + 1.75\right] * \frac{(1-\alpha)^2 v\ LT_H}{\alpha^3 d_p \bar{T} C_p \Delta T_H} \quad , \tag{19}$$

where the factor 2.5 has been added to allow for pump inefficiency, heat exchanger and other small pressure drops arising from expansion, contraction, bends, etc. In Eq. (19), μ is the fluid viscosity, α is the bed porosity, and d_p is the particle diameter.

The third major source of irreversible entropy is that produced in heat transfer between the heat-exchange fluid and the porous-bed particles during the regenerative stages of the cycle. For a given stage

$$\dot{Q} = hA_c \Delta T_{GS} \quad , \tag{20}$$

with h the conductance, A_c the contact area of the bed, and ΔT_{GS} the temperature difference between the heat-exchange fluid and the solid. An expression for ΔT_{GS} can be obtained in terms of the quality of the heat exchange in the regenerative stages from

$$N_{tu} = (T_H - T_C)/\Delta T_{GS} \quad , \tag{21}$$

where N_{tu} is the number of heat transfer units.[12] The contact area of the bed is given by

$$A_c = \frac{6(1-\alpha)V}{d_p} \quad . \tag{22}$$

Combining Eqs. (13), (16), (20), (21), and (22), the rate ratio for irreversible entropy is given by

$$\frac{\dot{\Delta S}_{IRR}}{\dot{\Delta S}_H} = \frac{12h(1-\alpha)\ L\ (T_H - T_c)^2\ T_H}{d_p \bar{T}^2 N_{tu}^2 \rho v C_p \Delta T_H^2} \quad , \tag{23}$$

where a factor two has been included to account for both regenerative legs of the cycle.

The fourth source of irreversible entropy production is in the external cold and hot heat exchangers. In counterflow heat exchangers there are two unavoidable contributions of irreversible entropy, i.e., stream to stream ΔT and the frictional ΔP for each side.[13] If the thermal capacities, $\dot{m}C_p$, where $\dot{m}$ is the mass flow rate, are unbalanced, an additional irreversibility occurs. However, it is possible to reduce all of these contributions to a negligible amount if a big enough area and volume can be afforded. In the calculations the pressure drop has been included in Eq. (19) as part of the pump inefficiency and the temperature effect for a total $\dot{Q}$ transferred at $\bar{T}$ can be estimated by manipulating Eq. (13) in combination with $T\Delta S = Q$ to yield

$$\frac{\dot{\Delta S}_{IRR}}{\dot{\Delta S}_H}\ (\text{Heat Exchanger}) = \frac{T_{IN} - T_{OUT}}{\bar{T} N_{tu}} \quad . \tag{24}$$

Considering that each stage has a cold and hot exchanger, Eq. (24) has to be included twice. Good low-temperature exchangers on helium liquefiers have N_{tu}'s in the range of 50-100.

There will be small amounts of irreversible entropy production from friction in seals, inefficiency in the electric drive motor, eddy current heating, charging of the superconducting magnet, provision for parasitic cooling to 4.2K, and other miscellaneous sources. The miscellaneous entropy production was estimated as 10% of the total from all other sources.

The principal major sources of irreversible entropy, for which equations have been written, were added together for each stage of the liquefier, and the liquefier efficiencies calculated for a wide range of system variables. The heat-exchange fluids chosen were 1.0 MPa (10 atm) helium or hydrogen at the mean temperature of each stage. Hydrogen produces slightly better efficiencies, primarily because of its higher heat capacity per unit mass. In the calculation of the efficiency h is obtain from[14]

$$h = 0.21\ (\rho v C_p/\alpha)\left(\frac{2\rho v d_p}{3\mu(1-\alpha)}\right)^{-0.31}\left(\frac{C_p \mu}{\kappa}\right)^{-1} \quad . \tag{25}$$

the value of the N_{tu} for Eq. (23) was calculated from $hA_c/\dot{m}C_p$ but N_{tu} in Eq. (24) has been taken as 100. If the calculated N_{tu} was greater than 100, it was set to 100 for practical reasons. Selected values of the variables for each stage are shown in Table I. Those values were selected because they gave the highest efficiencies. The values of efficiency as calculated ignores the fact that the magnetic refrigeration actually provides refrigeration all along the regenerator which may reduce the irreversible entropy. The projected overall characteristics of a 20-K 20-W liquefier are presented in Table II.

The cooling power allows for the conversion from ortho to para in catalytic converters at each of the four heat exchangers. The volume of the refrigerator is estimated by taking six times the volume of the magnets plus 20% for the drive motor. The mass of the refrigerator includes magnetic material, magnets, Dewar drive motor plus gear box, etc., magnetic shielding around the whole dewar, and a 10% of the total miscellaneous contribution. The input power is calculated from the four-stage efficiency calculations and allows for a 90% efficiency in the drive motor.

TABLE I

EFFICIENCY RESULTS FROM A SECOND-LAW ANALYSIS OF A FOUR-STAGE MAGNETIC LIQUEFIER

$\bar{T}_c$(K)	Q_c(W)	$\nu(H)_g$	λ(W/mK)	$V_c(m^3)$	L(m)	α	Vel(m/s)	d_p(m)	f	N tu	η(%)
23	21.1	0.02	0.1	1.29×10^{-3}	0.11	0.75	0.017	1.0×10^{-4}	12.8	298	85.3
23	20.8	0.09	0.1	1.28×10^{-4}	0.05	0.45	0.132	1.0×10^{-4}	4.9	300	83.6
23	21.2	0.09	0.1	1.60×10^{-4}	0.07	0.55	0.121	1.0×10^{-4}	4.6	300	85.6
23	21.4	0.09	0.1	2.07×10^{-4}	0.11	0.65	0.125	1.0×10^{-4}	3.9	290	85.8
84	107	0.09	0.1	2.0×10^{-4}	0.03	0.45	0.188	1.0×10^{-4}	13.5	300	88.8
84	109	0.09	0.1	3.2×10^{-4}	0.07	0.65	0.190	1.0×10^{-4}	9.1	300	92.1
84	108	0.09	0.1	3.18×10^{-4}	0.09	0.65	0.247	1.0×10^{-4}	7.4	300	90.2
84	109	0.09	0.1	4.48×10^{-4}	0.09	0.75	0.152	1.0×10^{-4}	8.4	232	91.4
143	223	0.09	0.1	4.34×10^{-4}	0.05	0.65	0.221	1.0×10^{-4}	13.5	243	90.4
143	223	0.09	0.1	6.09×10^{-4}	0.09	0.75	0.246	1.0×10^{-4}	9.3	243	90.8
141	224	0.09	0.1	6.10×10^{-4}	0.11	0.75	0.300	1.0×10^{-4}	7.9	279	91.1
223	399	0.09	0.1	8.39×10^{-4}	0.05	0.75	0.212	1.0×10^{-4}	16.4	167	90.4
223	399	0.09	0.1	8.40×10^{-4}	0.07	0.75	0.296	1.0×10^{-4}	12.3	211	90.8

TABLE II

ESTIMATED CHARACTERISTICS OF FOUR-STAGE HYDROGEN LIQUEFIER

Cooling Power:	20 W at 20.4 K (0.7 ℓ/h)
Overall Refrigerator Volume:	$7.6 \times 10^{-2} m^3$ (76 ℓ)
Overall Refrigerator Mass:	166 kg (367 lbs)
Input Power Requirement:	557 W (0.75 HP)
Total Power Rejection @ 300 K:	621 W
Overall Efficiency:	54% of Carnot (20 - 300 K)

Although a comparison with existing gas refrigerators is somewhat unfair because no 20 - 300 K magnetic liquefier has yet been built, it is interesting to compare to see what potential payoffs are projected by the analysis. Comparing the data from Table II and that taken from Ref. 9, we see that this magnetic liquefier potentially offers a factor of ~ 7 increase in efficiency, a factor of > 10 decrease in volume, and a factor of > 3 decrease in mass, all at very low operating frequency, which should enhance reliability.

The second-law analysis indicates some of the key parameters, such as the axial conductivity and shows that for high efficiency it is difficult to operate at frequencies higher than about 1 Hz, since a gas is used as the heat-exchange fluid and the resultant large mass flow produces too much flow loss. The heat transfer in the porous bed must also be extremely good.

The credibility of these calculations is based on several similar calculations by others on gas-cycle systems which do predict the actual efficiencies very well.[6,8] It is not too surprising that the overall efficiency in magnetic liquefiers is higher because the major sources of inefficiency in gas-cycle refrigerators have been eliminated, namely the compressor, associated aftercooler and the expanders.

ACKNOWLEDGEMENTS

It is a pleasure to thank W. F. Stewart for several discussions about the work presented in this paper and to thank the referees for their constructive criticism.

REFERENCES

1. Stanley, W. L., "Some Cost, Energy, Environmental, and Resource Implications of Synthetic Fuels Produced from Coal for Military Aircraft," Rand Corporation Report P-5578 (February 1976).
2. Witcofski, R. D., "Comparison of Alternate Fuels for Aircraft," NASA Report NASA-TM-80155 (1979).
3. Nikolowsky, W. T. and Noggle, L. W., "The Potential of Liquid Hydrogen as a Military Aircraft Fuel," Int'l. J. Hydrogen Energy 1 449-460 (1976).
4. Hord, J., "Economics of Hydrogen," in Hydrogen, Its Technology and Implications, Vol. V, K. E. Cox and K. D. Williamson, Jr., eds. (CRC Press Inc., Boca Raton, Florida, 1979).
5. Parrish, W. R. and Voth, R. O., "Cost and Availability of Hydrogen," in Selected Topics on Hydrogen Fuel, J. Hord, ed., NBSIR-75-801 (1975).
6. Baker, C. R. and Shaver, R. L., "A Study of the Efficiency of Hydrogen Liquefaction," Int. J. Hydrogen Energy 3, 321-334 (1978).
7. Baker, C. R., "Economics of Hydrogen Production and Liquefaction updated to 1980," NASA Contractor Report 159161 (1979); also see NASA CR-132611, NASA CR-145077, NASA CR-145282.
8. Voth, R. O. and Daney, D. E., "H_2 Liquefaction: Effects of Component Efficiencies," Proc. of IECEC, Newark, Delaware, pp. 1156-1162 (Aug. 18-22, 1975).
9. Strobridge, T. R., "Cryogenic Refrigerators - an Updated Survey," NBS TN-655 (1974).
10. Truman, R. C. and Fine, P. C., "On the Irreversible Production of Entropy," Rev. Mod. Physics 20, 91-77 (1948).
11. Bird, R., Stewart N. and Lightfoot, E., Transport Phenomena (John Wiley and Sons, Inc., New York, 1960), pp. 200.
12. Kays, W. K. and London, A. L., Compact Heat Exchangers (McGraw-Hill, New York, 1984), Chp. 2.
13. Bejan, A., "The Concept of Irreversibility

in Heat Exchanger Design: Counterflow Heat Exchangers for Gas to Gas Applications," J. of Heat Transfer, 99, 374-380 (1977).

14. Coppage, J. E. and London, A. L., "Heat Transfer and Flow Friction Characteristics of Porous Media," Chem. Eng. Prog. 52, 57-65 (1956).